RESEARCH METHODS VOLCANICA

A scanning electron microscope–energy dispersive spectrometry (SEM–EDS) method for the quantitative analysis of common volcanic phases

Nathan L. Andersen*[α] and Heather Winslow[β]

[α] U.S. Geological Survey Cascades Volcano Observatory, Vancouver WA, USA.
[β] U.S. Geological Survey Hawaiian Volcano Observatory, Hilo HI, USA.

Abstract

In situ microanalysis by X-ray spectrometry is a fundamental geochemical technique for volcanology and the geosciences generally and typically performed using an electron microprobe (EPMA) equipped with wavelength dispersive spectrometers (WDS). The related technique of energy dispersive spectrometry (EDS), implemented using either EPMA or a scanning electron microscope (SEM), offers advantages in throughput, simplicity, and cost, yet has historically been relegated to qualitative tasks. We present a quantitative EDS procedure implemented using a W-source SEM and a moderate size silicon drift EDS detector applied to common volcanic materials. Glass and mineral standard data demonstrate that the accuracy and precision of this method is comparable to EPMA–WDS. We show that electron beam damage can be mitigated in volcanic glass through sample-specific optimizations without the need for a time-dependent intensity correction. Our implementation using a relatively inexpensive instrument can potentially increase the accessibility of high-quality, quantitative X-ray microanalysis of major and minor elements.

Keywords: SEM; EDS; Microanalysis; Volcanic glass; Thermobarometry.

Submitted: 2025-05-25 | Accepted: 2026-06-16 | Published: 2026-07-02

Editor: J. I. Farquharson | Production: G. N. Fabbro

1 Introduction

Electron beam instruments, the scanning electron microscope (SEM) and electron probe microanalyzer (EPMA), have been fundamental tools of volcanology and petrology, and geoscientists generally, for decades. Imaging by SEM provides rich textural information which may be coupled to compositional information through backscatter electron or cathodoluminescence intensity and X-ray analysis by energy dispersive spectrometry (EDS). The complementary technique of EPMA utilizes wavelength dispersive spectrometry (WDS) to effectuate in situ, generally non-destructive analysis of major and minor elements at spatial resolutions ranging from a few µm at typical accelerating potentials (15–20 kV) to as fine as a few hundred nm for low kV analysis [Saunders et al. 2014; Rinaldi and Llovet 2015; Yang et al. 2022]. Among the numerous volcanology applications of electron beam methods are morphological analysis of volcanic ash and tephra, textural observations and analysis of phase populations, chemical correlation of proximal and distal deposits [e.g. Lowe et al. 2017], mineral thermobarometry [e.g. Putirka 2008], and the determination of timescales derived from the chemical reequilibration of crystals [e.g. Costa et al. 2020].

Whereas EPMA–WDS has long been a workhorse of in situ chemical analysis for geo- and material scientists, EPMA instruments are expensive to acquire, operate, and maintain, and accordingly generally the exclusive purview of larger, well-resourced research institutions. The prospect of quantitative analysis utilizing comparatively ubiquitous SEM instruments has long been tantalizing; however, quantitative EDS remains substantially less common than WDS methods in the geosciences, owing in part to concerns about peak overlaps, pulse-pileup artifacts limiting the count rates that can be utilized in quantitative workflows, and possibly bias against the technique engendered by the traditional emphasis on "standardless" quantification [Ritchie et al. 2012; Newbury and Ritchie 2015]. Parallel advances in detector technology and spectral processing have mitigated some of the challenges of quantitative EDS analysis, facilitating the development of EPMA–EDS and SEM–EDS methods that produce accuracy and precision for the analysis of major (>1 wt.%) and minor (0.1–1.0 wt.%) elements on par with WDS analysis, even in matrices with challenging peak overlaps [Ritchie et al. 2012; Newbury and Ritchie 2015; 2019]. However, despite advantages in cost, simplicity, and potential throughput [Ritchie et al. 2012; Newbury and Ritchie 2019; Guyett et al. 2024], the application of quantitative SEM–EDS to volcanology problems remains relatively rare [Kuehn et al. 2011; Pamukçu et al. 2020; 2021; Guyett et al. 2024], engenders skepticism from the broader research community [Wilson et al. 2021], and generally remains relegated to qualitative and semi-quantitative tasks such as phase identification and X-ray mapping. Here we present the quantitative analytical procedure developed for the relatively low-cost, W-source SEM–EDS system recently installed at the U.S. Geological Survey (USGS) Cascades Volcano Observatory (CVO) supported by pyroxene, plagioclase, olivine, magnetite, ilmenite, and volcanic glass standard data. The goal of our work was to develop a method that operates within the confines of our instrument-specific software; however, the investigation of analytical and spectrum processing parameters should also prove useful to the implementation of SEM–EDS procedures more generally. Mineral and glass standard data demonstrate that our analytical routine yields data of comparable accuracy

* nandersen@usgs.gov

Table 1: Expected concentrations of analyzed oxides for the method verification standards [wt.%]

Reference material[a]	Source[c]	SiO_2	TiO_2	Al_2O_3	Cr_2O_3	FeO(T)	NiO	MnO	MgO	CaO	Na_2O	K_2O	P_2O_5
San Carlos olivine	SMS	40.81				9.55	0.37	0.14	49.42				
Springwater olivine	SMS	38.95			0.02	16.62		0.30	43.58				
fayalite, SMS	SMS	29.22	0.04			67.55		2.14					
olivine, MAC	MAC	40.49				8.83	0.40	0.14	50.14				
anorthoclase, SMS	SMS	66.44		20.12		0.20				0.87	9.31	2.35	
labradorite, SMS	SMS	51.25	0.05	30.91		0.46		0.01	0.14	13.64	3.45	0.18	
labradorite, MAC	MAC	55.28		28.10		0.34				10.43	5.30	0.55	
albite, MAC	MAC	68.31		19.91						0.10	11.47	0.21	
diopside, SMS	SMS	55.81		0.11		0.25		0.04	17.79	25.28	0.25		
chromium augite	SMS	50.48	0.51	8.03	0.85	4.71		0.12	17.32	17.30	0.84		
Kakanui augite	SMS	50.73	0.74	8.73		6.34		0.13	16.65	15.82	1.27		
enstatite, MAC	MAC	53.00	0.10	3.84	0.16	13.80		0.30	28.58	0.22			
magnetite, SMS	SMS		0.16		0.25	90.94			0.05				
ilmenite, SMS	SMS		45.70			46.54		4.77	0.31				
VG-2	SMS	50.81	1.85	14.06		11.84		0.22	6.95	11.12	2.62	0.19	0.20
tektite glass	SMS	75.75	0.50	11.34		4.90		0.11	1.51	2.66	1.06	1.88	0.00
Lipari	BJLJ	74.10	0.07	13.10		1.55		0.07	0.04	0.73	4.07	5.11	0.01
Sheep Track	BJLJ	61.60	0.24	17.60		4.55		0.13	0.12	1.09	8.19	5.34	0.04
Old Crow	BJLJ	72.10	0.30	12.50		1.62		0.05	0.28	1.43	3.66	3.56	0.04
interlab A[b]	BJLJ	76.89	0.09	12.32		1.38		0.04	0.02	0.55	3.53	5.05	
interlab B[b]	BJLJ	77.20	0.18	12.23		1.14		0.05	0.08	0.47	3.39	5.16	
interlab C[b]	BJLJ	55.81	1.00	19.57		5.45		0.28	0.82	1.92	8.93	5.60	0.27
interlab D[b]	BJLJ	77.30	0.06	12.81		0.75		0.07	0.09	0.74	3.66	4.40	
Panum[b]	BJLJ	76.88	0.07	12.71		0.93		0.04	0.02	0.53	3.97	4.79	0.01

[a] Additional reference material information is available in Supplementary Table S1.
[b] Expected concentrations reported normalized to 100% anhydrous.
[c] SMS: Smithsonian Microbeam Standards; MAC: Microanalytical Consultants; BJLJ: Dr. Britta J. L. Jensen, University of Alberta.
Data sources: Jarosewich et al. [1979, 1980a,b]; Kuehn et al. [2011]; Helz et al. [2014]; Jensen et al. [2021]; Britta J.L. Jensen, University of Alberta (2023) personal communication.

and precision to typical EPMA methods and offers flexibility for the analysis of beam-sensitive materials such as volcanic glass.

2 Methods and materials

All data were collected at CVO using a JEOL IT510 W-source SEM, an Oxford Instruments Ultim Max 40 mm^2 EDS detector, and the Oxford Instruments AztecLive (OIA) EDS software, version 6.0 SP2 [Oxford Instruments 2023]. A notable feature of the IT510 when employed for quantitative analysis is the large sample chamber and available configurable sample holder, which allows the simultaneous loading of multiple standard and sample mounts or thin sections. Mineral and pure oxide reference materials used for calibration and verification, summarized in Tables 1 and S1, are from the Smithsonian Microbeam Standards collection (SMS) or purchased from Micro Analytical Consultants (MAC). All materials were mounted in epoxy-filled wells in 25 mm-diameter brass or leucite disks, ground and polished flat using 1 µm diamond followed by 0.25 µm alumina for the final polishing steps, and coated with approximately 20 nm of carbon prior to analysis.

Our preferred protocol for mineral analysis utilizes an accelerating voltage of 15 kV, working distance of 10 mm, process time of 16 µs (software setpoint 6, see below), a beam current scaled to a dead-time of 45–55% (generally produced by a current of 2–3 nA), a 30 µm final aperture, and it applies the pulse pileup correction implemented in OIA. At these conditions, typical output count rates were 20–25 kilo-counts per second (kcps). Spectra are collected with 1.5 million total counts (typically acquired within 35 s live time) using 4048 channels with 5 eV per channel. As documented in the following sections, we explored a range of spectrum counts, process times, low-dead-time routines without pulse pileup correction, and standardized versus "standardless" quantification. The optimal values of these parameters will vary between instruments. Analysts are encouraged to consult the manufacturer's recommendations and perform a similar set of tests as presented in this paper when implementing a quantitative analytical routine. Analyses were generally performed using the "point and shoot" function whereby analysis areas are placed on an electron image of the current field of view as either points or polygons. We did not note a difference in data quality between point and polygon analyses, except for beam-sensitive materials as discussed below. Whereas "point and shoot" analyses may suffer from poor focus compared to analysis of an entire field of view at high magnification [e.g. Guyett et al. 2024], we found that focusing using the secondary electron image at several times higher than the analysis magnification—e.g. 1000× to 3000×, 128 µm × 96 µm to 42.7 µm × 32.0 µm field of view (FOV), for analysis at 500×, a 256 µm × 192 µm FOV—was sufficient to produce quality data using the "point and shoot" work flow as long as analytical spots were placed within 150 µm of the center of the field of view; this requirement is explored below. Analysis of glass followed the same general setup as minerals; however, we investigated several optimizations to mitigate Na-mobility as detailed below.

OIA utilizes the measurement of the count rate on a pure metal as a proxy for beam current to calculate unnormalized

concentrations for both standardized and "standardless" quantification. We utilized a Co metal standard for these measurements due to its relative ease of polishing and resistance to oxidation compared to other metals. Beam measurements were performed every 10–20 min to establish beam stability at the start of each analytical day, then approximately every hour thereafter. Once stability is achieved, the beam measurements typically drift by <1% per hour, which is sufficiently stable to effectuate quantitative analysis. During most of the method development, the CVO SEM was not equipped with a probe current detector, so the current was set by targeting a preferred dead-time and comparing the Co count rates. The recent installation of a probe current detector has allowed us to retroactively calculate the beam current for past analytical sessions based on the Co count rate. Our typical analytical set up for minerals uses a current of 2–3 nA.

Calibration standards were run at the start of each analytical session (typically 1–3 d). We found that the calibration is stable for all elements for at least three days, and some elements were stable for months, though we did not systematically investigate the relative calibration stability of different elements. Whereas this report includes only standard analysis, for an analysis session including unknowns, three replicates of secondary verification standards are run following calibration and at the start of each day if utilizing a previous day's calibration; in either case additional replicates are run throughout the day to monitor the stability of the calibration. Typically, a total of 6–10 analyses will be measured daily for each secondary standard. We prefer to reserve our closest matrix-matched standards for secondary verification rather than utilizing them for calibration (Supplementary Table S1). A summary of the considerations and our suggestions for developing a SEM–EDS procedure are in the appendix.

3 Method validation and analytical conditions optimization

The following subsections document the optimization of our mineral analytical protocol. In addition to the figures presented in the text, tables summarizing the results of each test are available in the supplementary materials and Zenodo data repository [Andersen and Winslow 2026]. For each test, we analyzed 20 replicates each of the SMS labradorite and chromium augite and MAC olivine standards, except as noted. Throughout this report, results are reported as unnormalized wt.% oxides calculated using stoichiometric oxygen, unless otherwise stated.

3.1 Beam Stability

We observed significant beam current instability if we began analysis immediately after a sample change, which improved over time, reaching a stable state after approximately three hours. We mitigated this requirement by loading samples the night before analysis and allowing them to pump down overnight. After pumping overnight, the beam current usually stabilized after 30–60 min. We initially suspected that the additional pumping was required to achieve a better vacuum beyond that registered as a "high-vacuum" state by the SEM software, perhaps exacerbated by the large sample chamber of our SEM. However, the Tescan MIRA field emission source SEM at the USGS Alaska Volcano Observatory (AVO) has a similarly large sample chamber yet requires neither additional pumping nor stabilization time after turning the beam on (Matthew Loewen, U.S. Geological Survey, 2025, personal communication). Other than the source type, a critical difference between the CVO and AVO instruments is that the source of the CVO SEM vents during sample exchanges whereas the source of the AVO SEM is maintained at high vacuum. Accordingly, in addition to differences between the source type, we infer that venting, and potentially subsequent outgassing of the filament, is the most substantial contributor to the extra pumping and filament warm-up time required by the CVO SEM. Accordingly, we expect that the beam stability will vary, perhaps significantly, between models of SEM, and, to a lesser extent, between individual instruments of the same model.

The beam current typically became unstable during the 60–90 min prior to a filament burnout; however, we have not found any other effect of filament age on the performance of the method. We aim to tune the source power, bias, and alignment at least weekly when our SEM is being used regularly. Frequently, although not universally, we tuned the source when loading samples the night before or the morning before beginning a quantitative analysis session—the latter of which may also contribute to the need to "warm up" the source. We did not note a degradation in the method performance that is correlated to the time since the last tuning of the instrument; however, we did not investigate this systematically nor do we have data from conditions we would consider poorly tuned for comparison.

3.2 Total spectrum counts

We evaluated the effect of counting time by comparing spectra with 0.25×10^6–2.5×10^6 total counts; all were collected at an accelerating voltage of 15 kV, current of 2.2 nA, a dead-time of 45–55%, process time of 16 µs (software setpoint 6, see below), and include pulse pileup correction. Increasing the count time has a more substantial impact on the precision of the analysis than the accuracy (Figure 1; Supplemental Table S3). For the major elements, reasonable precision (relative standard deviation, rsd <2%; rsd = 100 × standard deviation/mean) can be obtained for spectrum counts as low as 0.5×10^6, though longer counting times do continue to improve the precision with diminishing returns beyond 1×10^6–1.5×10^6 total counts. For the minor elements, spectrum counts fewer than 1×10^6 yield poor precision (rsd > 40%). As observed for the major elements, diminishing returns begin for spectra with more than 1×10^6–1.5×10^6 counts, but longer counting times continued to produce notable improvement in precision for some minor elements of interest: the rsd of NiO in the MAC olivine standard (expected concentration = 0.4 wt.%) improved from 16.0% for 1.5×10^6 total counts to 13.8% for 2.5×10^6 counts; however, the improvement was less dramatic for other elements, for example the rsd of Na_2O in the chromium augite standard (expected concentration = 0.84 wt.%) was 2.9% and 2.0% for 1.5×10^6 and 2.5×10^6 total counts, respectively. An important caveat is that long counting times can be detrimental to the analysis

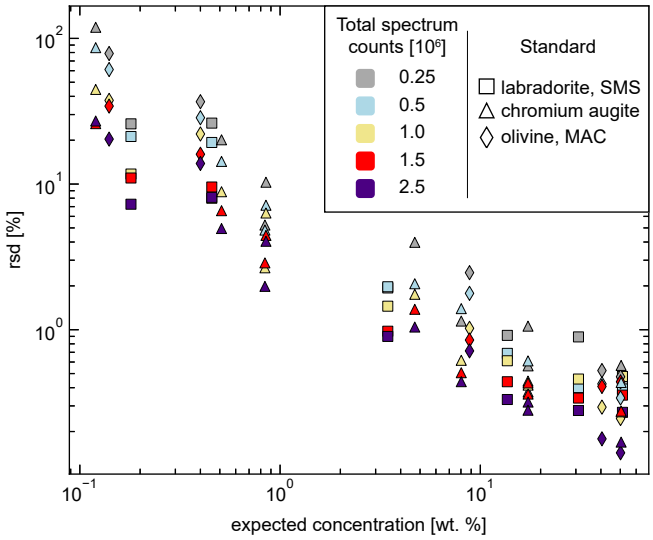


Figure 1: Comparison of the precision (relative standard deviation, rsd = 100 × standard deviation/mean) of standard measurements produced by spectra with total counts ranging from 0.25×10^6–2.5×10^6. We find significant diminishing returns to spectra with more than 1×10^6–1.5×10^6 counts for most elements. For each symbol, the total spectrum counts are indicated by the fill color and the standard by the shape. SMS: Smithsonian Microbeam Standards; MAC: Microanalytical Consultants.

of beam-sensitive materials, as discussed below. Accordingly, our "baseline" method is to measure spectra with 1.5×10^6 total counts—generally achieved by 35 s live time at our preferred conditions; however, if minor element concentrations are of particular interest for the project, longer counting times may be worth investigating.

3.3 Process time

We tested the effect of process times ranging from 0.5 to 16 µs on the spectral resolution; OIA implements the process time as a set of unitless, whole number set points (sp) ranging from 1 to 6. We collected spectra comprising 1.5×10^6 counts on the pure Si, pure Al_2O_3, Kakanui hornblende, and pyrolusite standards using a constant current of 3 nA such that the lower process times yielded a lower dead-time and higher output count rate, a working distance of 10 mm, and accelerative voltage of 15 kV. The resolution was measured as the full width half maximum (FWHM) of the major element peaks for each standard. For all peaks, increasing the process time from 0.5 µs (sp 1) to 3 µs (sp 4) produced substantial improvements in the resolution (Figure 2; Supplementary Table S8). There are diminishing returns in resolution improvement for the highest process time settings, 7 µs (sp 5) and 16 µs (sp 6), but the improvements are more substantial for the lower energy peaks (≤1.74 keV, Si K). Whereas increasing the process time from 3 µs (sp 4) to 16 µs (sp 6) improved the resolution of the Mn K peak, the highest energy in our test, by only 3.4%, the Na K peak resolution improved by 13.6%.

We tested the practical effect of this improved resolution by measuring mineral standards using process times rang-

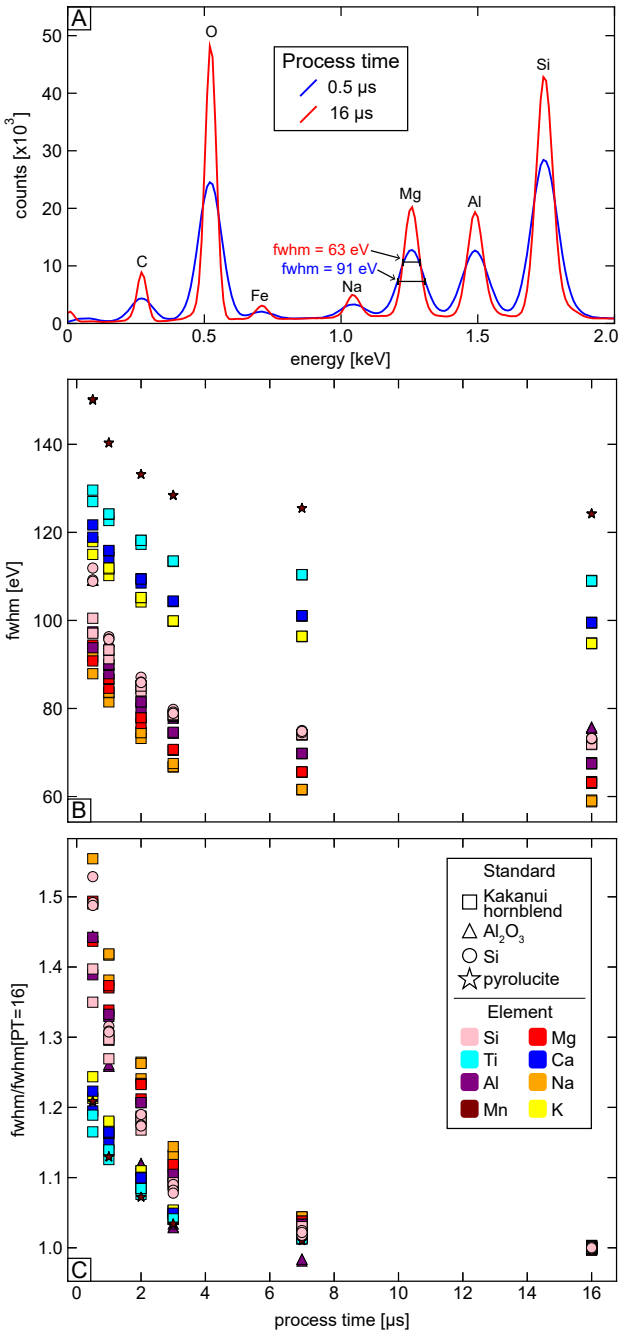


Figure 2: The effect of process time on the spectral resolution, expressed as the peak full width half maximum (FWHM). [A] Example of the low-energy end 0–2 keV) of spectra collected on the Kakanui hornblende at process times of 0.5 µs (blue) and 16 µs (red) illustrating the improved peak resolution, for example, a 31% improvement in the FWHM of the Mg peak. [B] The measured FWHM for each peak. [C] The FWHM of each peak normalized to that measured at a process time of 16 µs. Whereas the highest process time settings produce minor resolution improvements for the higher energy peaks, the low energy peaks continue to benefit. This is further reflected in improvements in the accuracy of these elements in standard measurements at the highest process time settings (see text and Supplemental Table S3). For each symbol, the element is indicated by the fill color and the standard by the shape.

ing from 2 µs (sp 3) to 16 µs (sp 6) and collecting spectra of 1.5×10^6 counts. We scaled the current to produce dead-times of 40–50% for process times >3 µs (sp 4); achieving this dead-time at a process time of 3 µs would have required excessive current, and therefore those measurements were performed at a dead-time of approximately 30%. Pulse pileup correction was applied to all measurements. While increasing the process time to 7 µs or 16 µs (sp 5 and 6) did not universally improve the accuracy of the measurements, analysis at the highest process time setting did produce substantial improvements in the relative percent difference (rpd = 100 × |measured − expected|/expected) of the mean measured concentrations relative to the expected values for Al and Fe in plagioclase, Mg and Na in pyroxene, and Fe in olivine (Figure 3; Supplemental Table S3). Taken together, we found 3 µs (sp 4) to be the minimum viable process time for quantitative analysis. At the longest process time setting, 16 µs, the analysis time is approximately 70 s, compared to 17 s at 3 µs (sp 4), which we judged to be tolerable to achieve the improved accuracy. However, we note that our experience is not universal, even among the Oxford Instruments Ultim Max line of detectors. For example, the two Ultim Max 100 mm^2 detectors recently installed at the USGS Alaska Volcano Observatory were tuned by the vendor to a different process time curve, 0.1–7 µs, and do not show any significant improvement in resolution or accuracy for process times greater than 1 µs (Matthew Loewen, U.S. Geological Survey, 2025, personal communication). Accordingly, the effects of the process time on the resolution and accuracy should be assessed for each instrument.

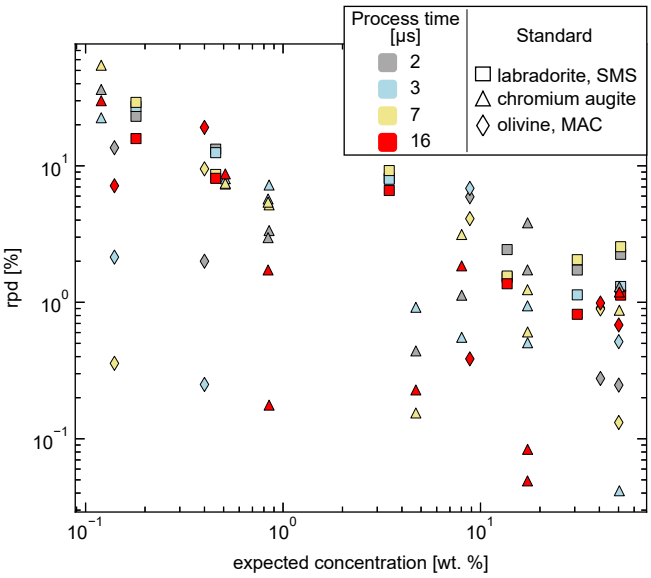


Figure 3: Comparison of the accuracy as relative percent difference (rpd = 100 × |measured − expected|/expected) of standard measurements produced at process times of 2–16 µs. The analysis of several (e.g. Al and Fe in plagioclase, Mg and Na in pyroxene, and Fe in olivine), but not all (e.g. Si in plagioclase, pyroxene, and olivine), elements benefits from the longest process times. For each symbol, the process time is indicated by the fill color and the standard by the shape. SMS: Smithsonian Microbeam Standards; MAC: Microanalytical Consultants.

3.4 Lateral consistency

Most commercial EDS software, including OIA, implements a "point and shoot" analysis workflow whereby the user acquires an SEM image that is then used as a map for placing analysis locations. The spectrum for each location is then collected by deflection of the beam. This contrasts with typical EPMA workflows whereby each target spot is relocated to a fixed beam. We tested the consistency of the spectra acquired across a 512 µm × 384 µm FOV (250× magnification) and a 256 µm × 192 µm FOV (500× magnification)—moderate magnifications that are typically appropriate for imaging major phenocrysts. We measured profiles across a homogeneous olivine standard using 15 kV, a 3 nA current, 35 s live time for each spot, process time of 16 µs, and spot spacing of 15 µm or 30 µm. In the 512 µm × 384 µm FOV, significant variations in the Mg count rate are present on the outer 50–100 µm of the 450–600 µm profiles; however, the ratio of the Fe and Mg counts stayed consistent despite the systematic spatial variation in count rate (Figure 4). For the 256 µm × 192 µm FOV, the Mg count rate and Mg/Fe ratios are consistent across the entire 300 µm (diagonal) FOV. Our preferred method is to perform analyses in a FOV no larger than 256 µm × 192 µm—i.e., at magnifications of at least 500×; however, this test demonstrates that consistent results are also obtained by beam deflection within an approximately 150 µm radius of the center of the SEM field of view, corresponding to the optimal field of view of the EDS detector collimator, at lower magnifications.

3.5 Pulse pileup correction

One of the limiting factors of traditional quantitative EDS analysis is pulse pileup artifacts that result when multiple x-rays are detected close in time such that the counting electronics conflate them as a single event with an energy equal to the sum of all the coincident X-rays. The result is not only the generation of spurious sum peaks, but also the loss of signal from the characteristic energy peaks of interest. The frequency of pileup events increases with dead-time, which typically limits the throughput of EDS analysis as the current/count rate is lowered to maintain a dead-time of <10% [Ritchie et al. 2012]. To address this difficulty OIA implements a pulse-pileup correction which identifies peaks resulting from pileup events, removes them from the spectrum, and adds those counts back to the appropriate characteristic energy peaks. To test the robustness of this correction, we performed a set of standard analyses using a process time of 7 µs and current of 2.2 nA resulting in a deadtime of approximately 5%. We found no significant improvement in the accuracy of results using this uncorrected, low dead-time approach compared to the high dead-time approach utilizing the pulse-pileup correction (Supplemental Table S3). Moreover, the low dead-time approach effectively precludes analysis using our highest process time set point as the analysis times become impractically long for supervised analyses—approximately 200 s for the 2 nA and

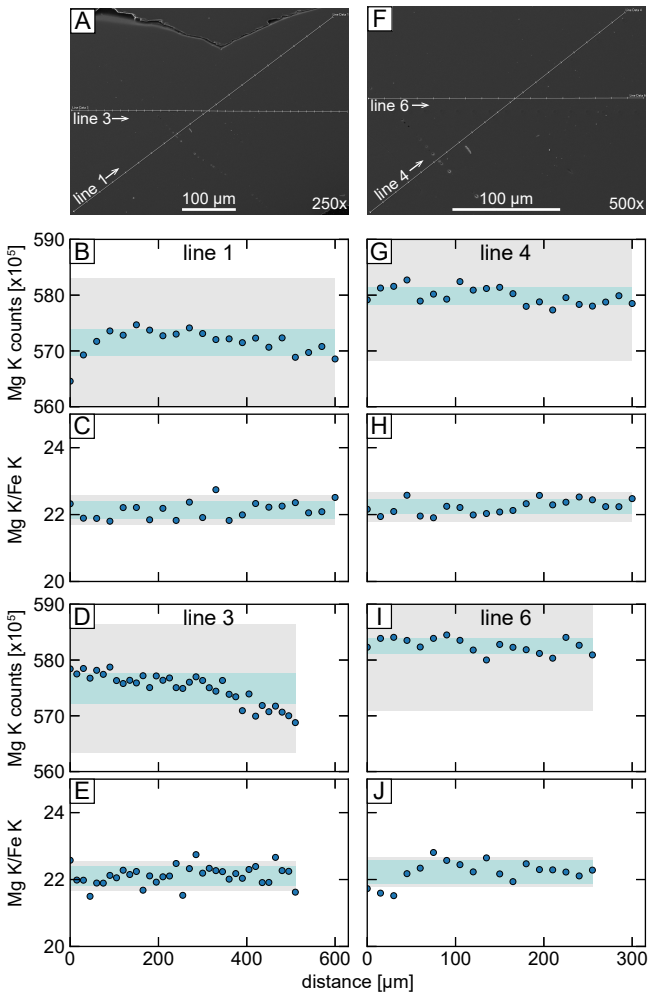


Figure 4: Line scans on the MAC olivine standard showing variation across the field of view (FOV) at 250× (512 µm × 384 µm FOV; left column) and 500× (256 µm × 192 µm FOV; right column). [A] and [F] The orientation of the line scans in secondary electron images. The blue fields show two standard deviations about the mean, and the gray field shows the mean ±4%. Whereas some variation in the count rate is observed on the outer margins of the 250× FOV, taken together, these results indicate the analysis by beam deflection within an approximately 150 µm radius of the center of the FOV has no adverse impact on the data quality.

7 µs process time runs. Long analysis times can also degrade the accuracy of some elements and be detrimental to the analysis of beam-sensitive materials, as discussed below. Accordingly, our preferred approach is to utilize the pulse pileup correction to achieve higher throughput.

3.6 Selection and homogeneity of calibration standards

The structure and workflows of commercial EDS software generally favor the use of a single set of calibration standards for a range of matrices. Whereas modern matrix corrections utilized in X-ray microanalysis have substantially reduced the need to closely match the matrix of the calibration standards and unknowns, we nevertheless found that some elements were sensitive to the choice of calibration standard. Moreover, for the case of natural mineral reference materials, standard materials are not always strictly homogeneous, and the expected values of standards may not be perfectly intercalibrated. Accordingly, the analysis of several standards of the same matrix can reveal that while one calibration standard may produce the "best" results for a particular standard, another may yield the best compromise for several standards.

When evaluating the results over time, we found that the Na_2O measurements of the SMS labradorite standard (expected Na_2O concentration = 3.45 wt.%) yielded an anomalously high rpd of 7.6% when Na was standardized using the MAC albite standard. Restandardizing using the MAC jadeite improved the rpd to 3.3%; however, we also found that the three grains of the SMS labradorite we analyzed did not produce consistent results (Figure 5). Grain 4 produced a mean of 3.49 ± 0.06 wt.% (rpd = 1.3%) versus 3.64 ± 0.05 wt.% (rpd = 5.5%) for grains 1 and 3, both calculated relative to the MAC jadeite. Calibrating instead with the albite standard yields results 5.4% and 3.0% higher (rpd = 6.6% and 8.8%), respectively. The MAC labradorite (expected Na_2O = 5.3 wt.%) yields a similar trend with the albite standardization producing mean Na_2O concentrations 4.7% higher than the jadeite standardization, 5.39 ± 0.12 wt.% (rpd = 1.6%) versus 5.15 ± 0.06 wt.% (rpd = 2.9%). However, in contrast to the SMS labradorite, the MAC labradorite yields a lower rpd when Na is calibrated using the albite standard versus the jadeite standard.

The An contents of the SMS and MAC labradorite standards, An_{68} and An_{50} (An = 100 × Ca/[Ca + Na + K] on a molar basis), span the interval of An_{50}–An_{70} where plagioclase undergoes a significant structural transition from I1 to C1 due to a change in the ordering of Al [Carpenter and McConnell 1984]. Whereas the An content at which this transition occurs within this range is temperature-dependent, and the temperatures at which these standard materials crystallized are unknown, most likely the MAC standard has the C1 structure and the SMS standard the I1 structure. Accordingly, the difference in the accuracy of these standard results for the two Na calibrations is indicative of a matrix effect related to this structural transition. The jadeite standard may be preferable for higher An plagioclase and the albite for lower An. However, we cannot strictly rule out that this difference results simply from the imperfect intercalibration of the standards. When analyzing unknowns, quality controls for the samples, such as the oxide total, stoichiometry, and charge balance, should also be considered when selecting the optimal calibration standard.

We tested four calibration standards for Mg in olivine and pyroxene: SMS chromite, MAC diopside, MAC enstatite, and Springwater olivine. For two olivine and two pyroxene standards, these calibrations yielded the same relative trends in MgO concentrations, diopside produced the highest MgO and Springwater olivine the lowest (Figure 5). However, for olivine, the high concentrations produced by the diopside standardization yielded rpd >2% with the Springwater olivine and enstatite standardizations producing the lowest rpd. In contrast, the Springwater olivine standardization produced the highest rpd for each pyroxene standard and diopside an rpd <2% for each. In this case, despite producing the lowest rpd

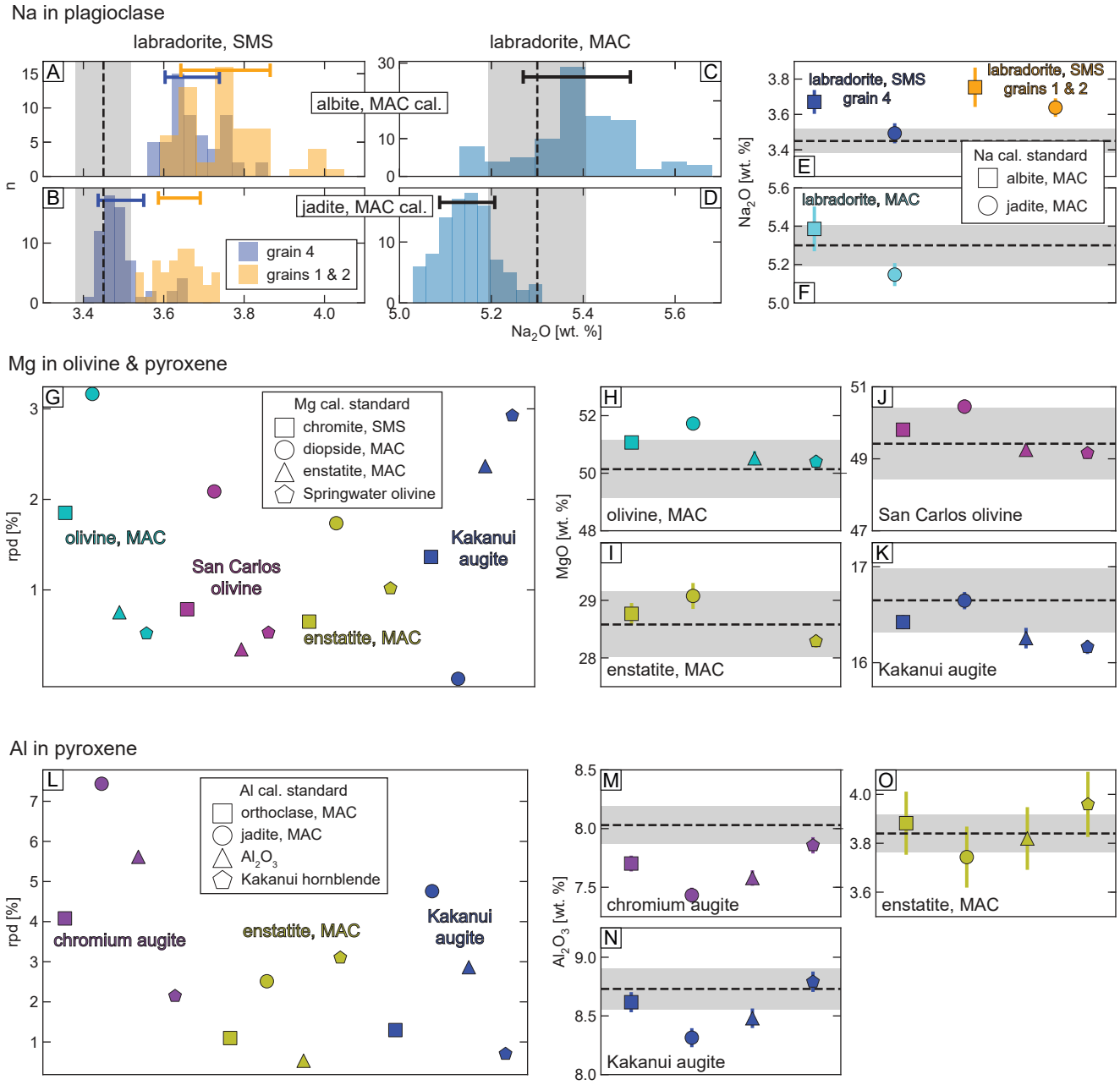


Figure 5: Examples of the evaluation of standard intercalibration and standardization matrix optimizations. The dashed lines and gray boxes are the expected concentrations with a 2% confidence bound. Error bars are ±1 standard deviation and often smaller than the symbols. [A–F] Na in plagioclase. Repeated analysis of the Smithsonian Microbeam Standards (SMS) labradorite showed it to be heterogeneous at the grain scale [A, B]. The albite and jadeite calibrations produced similar relative Na_2O concentrations for both labradorite standards; however, the jadeite standardization produced better accuracy for the lower-Na SMS labradorite, whereas the albite standardization was more accurate for the higher-Na Microanalytical Consultants (MAC) labradorite. [G–K] Mg in olivine and pyroxene. All Mg calibrations produced the same relative trends in MgO in the olivine and pyroxene data. [L–O] Al in pyroxene. As with Mg, the standardizations produced consistent relative Al_2O_3 concentrations. In all cases, the differences in the accuracy produced by the calibration standards are indicative of matrix effects; however, imperfect intercalibration of the standards cannot be strictly ruled out.

for only one of the standards, the chromite standardization provides the best compromise if a single MgO calibration is desired for both olivine and pyroxene as it yields an rpd <2% for all standards considered in this test.

We found similar trends for the analysis of Al in pyroxene. We tested calibrations using MAC orthoclase, MAC jadeite, pure Al_2O_3, and the Kakanui hornblende. As with Mg in olivine and pyroxene, these four calibrations produced consistent relative Al compositions with jadeite yielding the lowest concentrations and Kakanui hornblende the highest. Somewhat counterintuitively, jadeite produces the worst accuracy of these calibrations. The enstatite standard was relatively re-

silient to the choice of calibration. All four yielded means within one standard deviation with rpd = 0.5–3.1%. The Kakanui and chromium augite standards were more sensitive to the Al calibration. The Kakanui hornblende standardization produced the most accurate results for both whereas this standardization was nominally the least accurate for enstatite. Accordingly, our results indicate that the Kakanui hornblende is preferred for higher-Al clinopyroxene analysis, whereas the orthoclase calibration is preferred for lower-Al orthopyroxene; either the orthoclase or Kakanui hornblende calibration would be a reasonable choice as a compromise Al standard for mixed pyroxene unknowns. On the other hand, we found the jadeite and Al_2O_3 calibrations yield inaccurate results for the augite standards and are best avoided for Al calibration for pyroxene analysis.

Taken together, these examples show that the choice of calibration standard can produce subtle, but resolvable differences in the measured compositions. In our experience, it is generally possible to find a compromise set of standards that will produce acceptably accurate results for several phases, but that an optimized standardization for each phase will generally produce improved accuracy for some elements. Moreover, while some of our results could reflect of matrix effects, we cannot rule out that the standards are simply neither perfectly intercalibrated nor homogeneous, which is likewise a concern for EPMA–WDS analysis particularly when employing natural reference materials [e.g. Fournelle 2011; Harries 2014; Allaz et al. 2015; Fournelle et al. 2020]. Accordingly, we have found it useful to run multiple representative secondary standards when possible to avoid tailoring the calibration too much to the expected concentrations of a single standard.

3.7 Comparison to "standardless" analysis

Traditional "standardless" approaches to EDS analysis utilize a library of standard spectra for quantification, often supplied by the detector vendor. Traditionally, one of the most significant drawbacks of "standardless" quantification is the need to normalize the results to 100% total oxides, which eliminates one of the principal criteria for judging data quality. By using the count rate on Co as a proxy for beam current, OIA calculates unnormalized "standardless" results thereby eliminating a substantial drawback of this approach. However, the accuracy is still dependent on the quality of the standard library and how closely the analysis conditions of the unknowns match the library conditions [Newbury and Ritchie 2015]. The optimal conditions for "standardless" analysis will vary based on the factory standard libraries provided by the manufacturer; OIA includes standard libraries recommended for analysis at a working distance of 10 mm using accelerating potentials of 20 kV and 5 kV. We performed analysis of plagioclase, pyroxene, and olivine standards at 15 kV and 3 nA and 20 kV and 2 nA and quantified each set using laboratory standards measured at the same conditions as the unknowns and using the 20 kV factory standard set (Figure 6; Supplementary Table S3). A lower current was employed at 20 kVto maintain a dead-time of 40–50%. We find that standardless analysis at 20 kV, including the beam energy measurement on the Co standard, offers accuracy in many cases comparable to standardized analysis such that it can be a viable approach for at least some geologic applications.

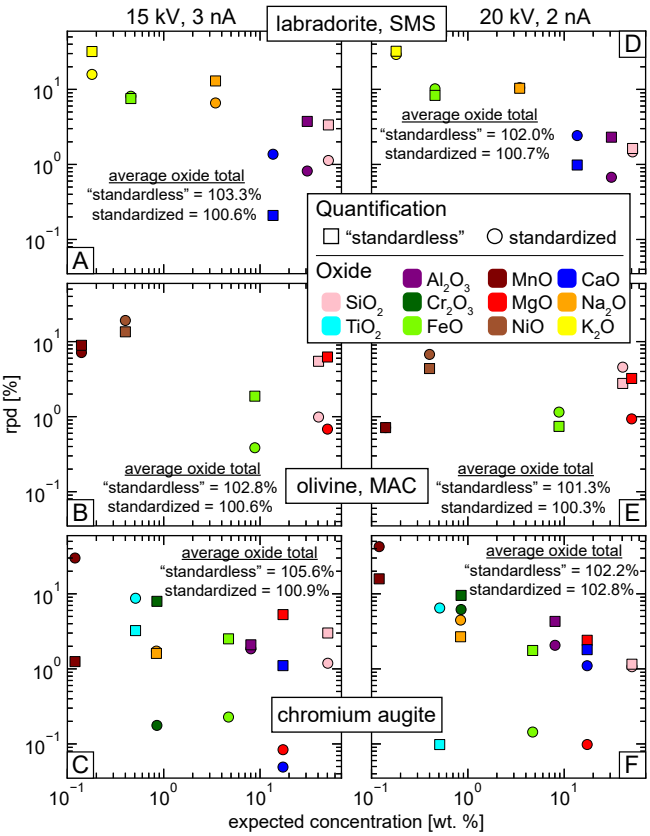


Figure 6: Comparison of standardized (circles) and "standardless" (squares) quantification—using the 20 kV standard library included in the Oxford Instruments AzTec software [Oxford Instruments 2023]—at 15 kV and 3 nA [A–C] and 20 kV and 2 nA [D–F]. The symbol fill color indicates the oxide. The "standardless" results at 20 kV produce a level of accuracy sufficient for research applications; however, the analytical totals are higher than ideal. When collected at a different accelerating voltage than used to collect the factory standard data, e.g. 15 kV, the accuracy of the "standardless" analyses degrades and the analytical totals become quite high. Relative percent difference, rpd = 100 × |measured − expected|/expected.

However, at 15 kV, standardized analysis offers substantial advantages in accuracy compared to "standardless" analysis. The rpd of the standardized analysis is 2–6× lower for Si and Al in plagioclase, Si, Mg, and Ca in pyroxene, and Si and Mg in olivine. The "standardless" analysis also yielded high totals, averages of 103.1 wt.%, 102.8 wt.% and 105.6 wt.%, for the plagioclase, pyroxene, and olivine standards, respectively, compared to 100.6 wt.%, 100.6 wt.% and 101.6 wt.% for the standardized analysis (Supplemental Table S3). Moreover, an accelerating voltage of 15 kV is often preferred for the analysis of silicate and oxide minerals as it provides a reasonable trade-off between the X-ray excitation of the elements of interest and the size of the X-ray generation volume [Yang et al. 2022]—the latter of which is a critical consideration when at-

tempting analysis of finely zoned minerals, small inclusions, or vesiculated matrix glass.

Whereas standardless analysis in theory provides a simplified approach to quantitative analysis, acquiring geologically interpretable data requires performing the beam energy measurement and the analysis of secondary verification standards, and thus does not relieve the analyst of the effort of sourcing standards nor of using a large sample holder or sample exchanges to measure standards. The analysis of a full set of calibration standards typically requires less than one hour; accordingly, we find that the additional accuracy and flexibility of standardized analysis is worth the relatively minor additional effort required.

3.8 Long-term reproducibility of mineral standards

The accuracy and precision of pyroxene, olivine, magnetite, ilmenite, and feldspar standards was evaluated using data acquired during multiple sessions from May 2023 to April 2025 (Figure 7). The accuracy and precision of the standard results are comparable to typical EPMA methods as shown by the consistency of our standard results. For all major elements except MnO, the rpd is <5% and is <2.5% for nearly all standards (Figure 7; Supplementary Table S5). MnO is present in major element levels in the SMS fayalite and SMS ilmenite standards (expected = 2.14 wt.% and 4.77 wt.%, respectively) and yields elevated rpd of 6.3% and 4.5%. In each case, the rsd is consistent with other analytes of similar concentrations indicating that heterogeneity of the standard is not likely the source of the inaccuracy. Standards with MnO concentrations <1 wt.% yield accuracy consistent with other elements of similar concentration. The MnO analyses of the fayalite and ilmenite standards were each calibrated using the other and therefore we conclude that the elevated rpd most likely reflect imperfect intercalibration of these two standards. The rpd of minor elements generally increases from approximately 5 to 30% for elements of concentration 1 to 0.1 wt.%.

The rsd of the major elements are mostly <2%, a handful are 2–5% for concentrations of 1–10 wt.%, and are 3–30% for the minor elements. The rsd varies from approximately 3–5% for concentrations of 0.7–1 wt.% to approximately 30% for those of 0.15–0.2 wt.%. The rsd is strongly corelated with concentrations for all elements in all standards, with a slightly weaker correlation for the highest concentration measured. In contrast, the rpd shows a general correlation with expected concentration but significantly more scatter. Neither the rpd nor rsd is correlated to the atomic number of the element.

In addition to the standard data reported here, analysis of unknown samples during this time period yielded consistently acceptable oxide totals (100 ± 2% for nominally anhydrous phases without substantial Fe^{3+}) and stoichiometry (total formula cations ±0.03 of expected). Several unknown samples were measured by both EPMA–WDS and SEM–EDS or could be compared to published EPMA datasets; the SEM–EDS method produced results consistent with EPMA both for the concentrations of individual spots as well as derived parameters, for example, Fe–Ti oxide temperatures and orthopyroxene Fe–Mg diffusion timescales [Andersen et al. 2025; Winslow et al. 2025].

4 Analysis of beam-sensitive materials

The migration of ions in beam-sensitive materials is a well-known difficulty with electron beam methods. This effect is particularly pronounced for the analysis of Na in hydrous volcanic glass [e.g. Kuehn et al. 2011; Iverson et al. 2017]. Beam damage may be mitigated by lowering the electron dose to the sample by increasing the analyzed area, decreasing the counting time, and/or lowering the beam current; however, Guyett et al. [2024] found that Na is mobilized by a beam current of only 300 pA during a one-minute analysis. EPMA methods may also implement a time-dependent intensity (TDI) correction to account for Na migration. TDI correction has not been implemented in any publicly available EDS software, so the Na migration must be mitigated by optimizing the electron dose.

We evaluated the mobility of Na and strategies for its mitigation in Na-rich feldspar and volcanic glass. Standards for these experiments are summarized in Table 1 and are from the SMS, the intercomparison study of Kuehn et al. [2011], the Panum crater obsidian of Jensen et al. [2021], which is equivalent material to standard OH-1 of Wu et al. [2022], and four samples from a yet unpublished interlaboratory comparison study (Britta Jensen, University of Alberta, 2023, personal communication). OIA does not have the capability to produce areas of a consistent, predefined shape, size, and aspect ratio in the "point and shoot" workflow. Rather, each area must be drawn by hand using a rectangle, ellipse, or freehand area tool. The dimensions of each rectangular and elliptical spot were confirmed using the feature measurement tool in the EDS software and the freehand areas were measured in exported images using image analysis software. The spot size for EPMA analysis is typically expressed as the beam diameter; we recast our spot sizes as the side length of a square of equivalent area, i.e., the square root of the raster area, so that the size of rasters with variable aspect ratio can be directly compared in terms comparable to typical EPMA procedures. We measured approximate square and circle rasters of 1.2–59 µm and rectangles with aspect ratios up to 4.6:1.

We initially tested if analyzing area rasters could mitigate Na mobility using our baseline mineral analytical setup. These analyses were performed at 15 kV, using a current of 2.5–3 nA, and collected 1.5×10^6 total counts, requiring an average analysis time of 63 s. Dead-times were 40–50% for spot analyses; analysis of area scans decreased the count rate, yielding dead-times of approximately 30% for the same current.

The Na-mobility behavior differed between two Na-rich feldspar standards, albite and anorthoclase. The albite standard yielded consistent Na_2O concentrations for the point analysis and all rasters. In contrast the anorthoclase measurements displayed apparent Na-loss for the point analysis, but a raster of only a few µm was sufficient to mitigate this effect (Figure 8).

For the glass standards, the nominally anhydrous, subalkaline, and mafic VG-2 standard yielded consistent Na_2O compositions for point analyses and all raster sizes, but all other glass standards displayed significant Na loss for the point and small raster analyses (Figure 8). All standards but the Sheep Track tephra, discussed further below, produced consistent

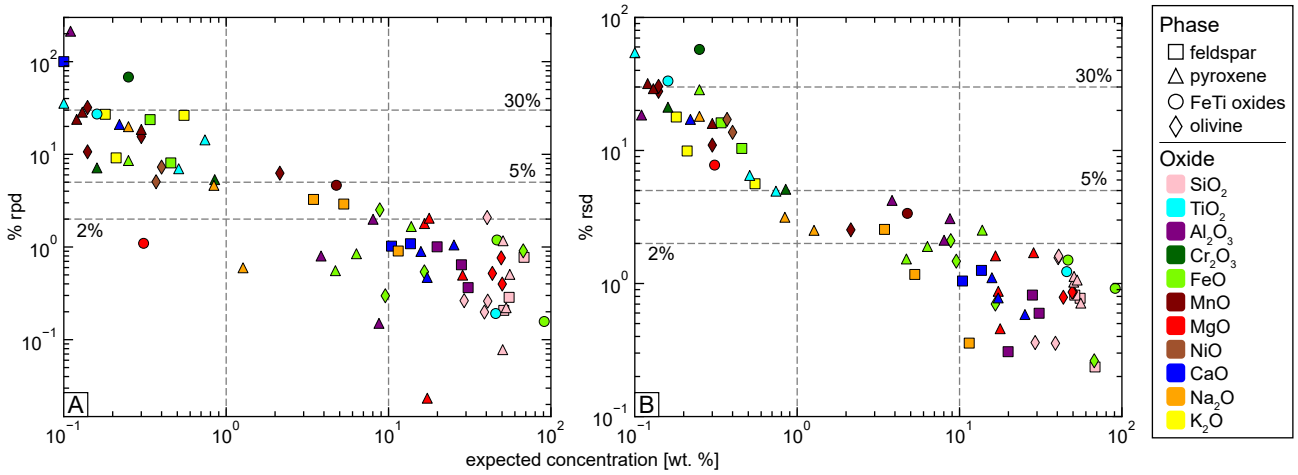


Figure 7: Summary of the accuracy and precision of nearly two years of mineral standard analyses. The symbol shape is the phase, and the fill indicates the oxide; the standards are listed with their expected concentrations in Table 1. [A] The relative percent difference (rpd = 100 × |measured − expected|/expected) compared to the expected concentrations. [B] The relative standard deviation (rsd = 100 × standard deviation/mean) of the measurements.

Na_2O with a raster size of at least 10 µm, and the Na_2O concentrations of some stabilized for spots as small as 5 µm. In addition to increasing the analysis area, decreasing the beam current may also mitigate Na mobility in glass. We measured an additional set of points and rasters for a subset of the glass standards utilizing a current of 0.6–0.7 nA, which required an average analysis time of 149 s to produce spectra with 1.5×10^6 total counts. Surprisingly, the relationship between raster size and Na_2O concentration was unchanged at the lower-current conditions.

To better delineate the effect of the beam current on Na-mobility, we analyzed points and 3 µm rasters on the Lipari standard using a process time of 3 µs (sp 4) and collecting 1.5×10^6 count spectra at currents ranging from 0.6 nA (dead-time = 3%, analysis time = 160 s) to 12.4 nA (dead-time = 53%, analysis time = 15 s). The Na_2O concentrations of the spot analysis increased from 2.35 wt.% at 0.6 nA to a maximum of 2.75 wt.% at 4.7 nA (expected Na_2O concentration = 4.07 wt.%), indicating substantial beam damage during point analysis and that any mitigating effect of the lower current was swamped by the longer analysis time. Further increasing the current produced slightly lower Na_2O concentrations, reflecting the diminishing returns in throughput as the dead-time increased (Figure 9). A similar, though smaller magnitude, trend was observed in the 3 µm rasters, which reached a maximum Na_2O concertation of 3.88 wt.% at 3.6 nA and 4.7 nA.

The Sheep Track tephra reference material is notable for being particularly vulnerable to beam-induced Na-loss [Kuehn et al. 2011], which is exacerbated by the fine particle size and vesicularity of our sample that limit that areas on which a large raster can be placed. These difficulties are reflected in our initial results for this material, shown in Figure 8, that don't reach a consistent Na_2O concentration over the range of rasters analyzed and all are significantly less than the consensus value. To improve our results for this material, we optimized the current by measuring points and 5 µm rasters over a range of currents. As with the Lipari reference material, we found that lowering the current too much was counterproductive; however, the best trade-off between the current and analysis time was somewhat lower current for Sheep Track, 3.2 nA, than for Lipari (Figure 9). We also evaluated the rate of Na-loss by making repeated analyses of the same 11.6 µm × 8.8 µm field of view (11 000× magnification) at 3–3.2 and 0.6 nA. At the higher current conditions, the acquisitions were 5 s; at 0.6 nA we made repeated 10 s analyses (the longer counting times were needed to produce sufficient precision for each analysis) and repeated 0.25×10^6 count acquisitions, which required approximately 27 s. We found substantial variability in the Na-loss response of the standard during these tests. For example, at 3–3.2 nA, stable Na_2O concentrations were observed for 40 s in one location, but substantial Na loss occurred after only 10 s in another (Figure 9). Similarly, the most stable test at 0.6 nA maintained a consistent Na_2O concentration for 40 s, but all tests of repeated 0.25×10^6 count analyses displayed substantial Na loss in the first step, i.e., after only 27 s. While we found similar timeseries of Na loss at the two current conditions, the output count rate at 3 nA is roughly double that at 0.6 nA, and we find that the higher current analysis always have higher cumulative counts for a given level of apparent Na loss and therefore decreasing the current becomes counterproductive as any mitigation of beam damage by the lower current is outweighed by the longer analytical times.

Informed by these tests, we conducted a new set of analyses at the optimized current with a live time of 5 s resulting in spectra of only approximately 0.25×10^6 counts. To increase the raster area, we used the free hand tool to select areas of arbitrary geometry in the "point and shoot" workflow (Figure 9). The resulting mean Na_2O concentration is in reasonable agreement with the consensus value (mean = 8.05 wt.%, expected = 8.19 wt.%, rpd = 1.7%, n = 11), if still slightly lower, but comes at the price of degraded precision for the minor elements (Figure 9; Supplementary Table S5).

Our experience with these materials demonstrates that the response to the electron beam can vary substantially for nat-

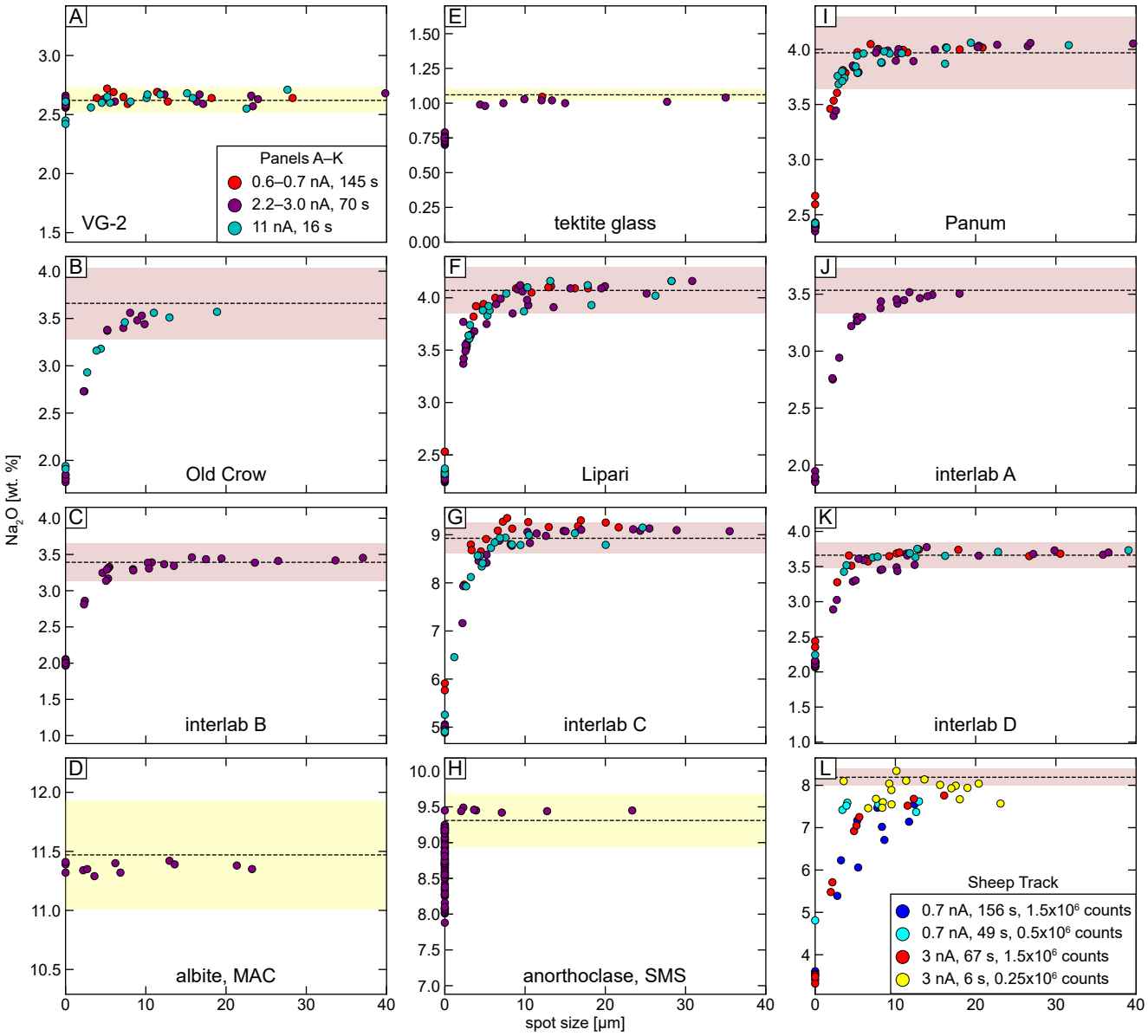


Figure 8: Summary of the effects of analytical area and current on the migration of Na in feldspar and volcanic glass. For [A–K], spectra with 1.5 × 10^6 counts were collected at 0.6–0.7 nA, 2.2–3.0 nA, and 11 nA; for the Sheep Track standard [L] analysis was performed at either 0.7 nA or 3 nA with analysis times and spectrum counts ranging from 6 s and 0.25 × 10^6 counts to 156 s and 1.5 × 10^6 counts (see text for additional details). The spot size is given as the width of a square of equivalent area (i.e., the square root of the area). Point analyses show significant Na-loss in all materials except for [D] albite and [A] VG-2, a nominally anhydrous basaltic glass. For most of the glass reference materials, rasters of 5–10 µm were sufficient to mitigate Na migration. The Sheep Track tephra [L] is more susceptible to beam damage and required optimization of the beam current and short counting times (see text for additional details). Pink fields show the standard deviation reported for the expected concentration and yellow fields are ±2% about the expected concentration for those reported without standard deviations. The data for the Panum obsidian and interlab A–D are plotted normalized to 100% for consistency with the expected concentrations.

ural samples. As shown by our analyses of the Sheep Track tephra, by measuring a range of raster sizes, the SEM–EDS method can quickly identify problematic samples so that additional mitigation strategies can be pursued. Despite no capability to apply a TDI correction, our results demonstrate that SEM–EDS analysis can mitigate Na-mobility at a spatial resolution comparable to or better than the beam diameters typically employed for EPMA analysis of glass—e.g. 6–20 µm [Iverson et al. 2017]. Instruments equipped with one or more large area detectors (e.g. ≥100 mm^2) should be able to maintain short analysis times at lower currents and thereby allow for the analysis of smaller areas and difficult samples without a loss of precision [e.g. Guyett et al. 2024]; however, such detector configurations are significantly more expensive.

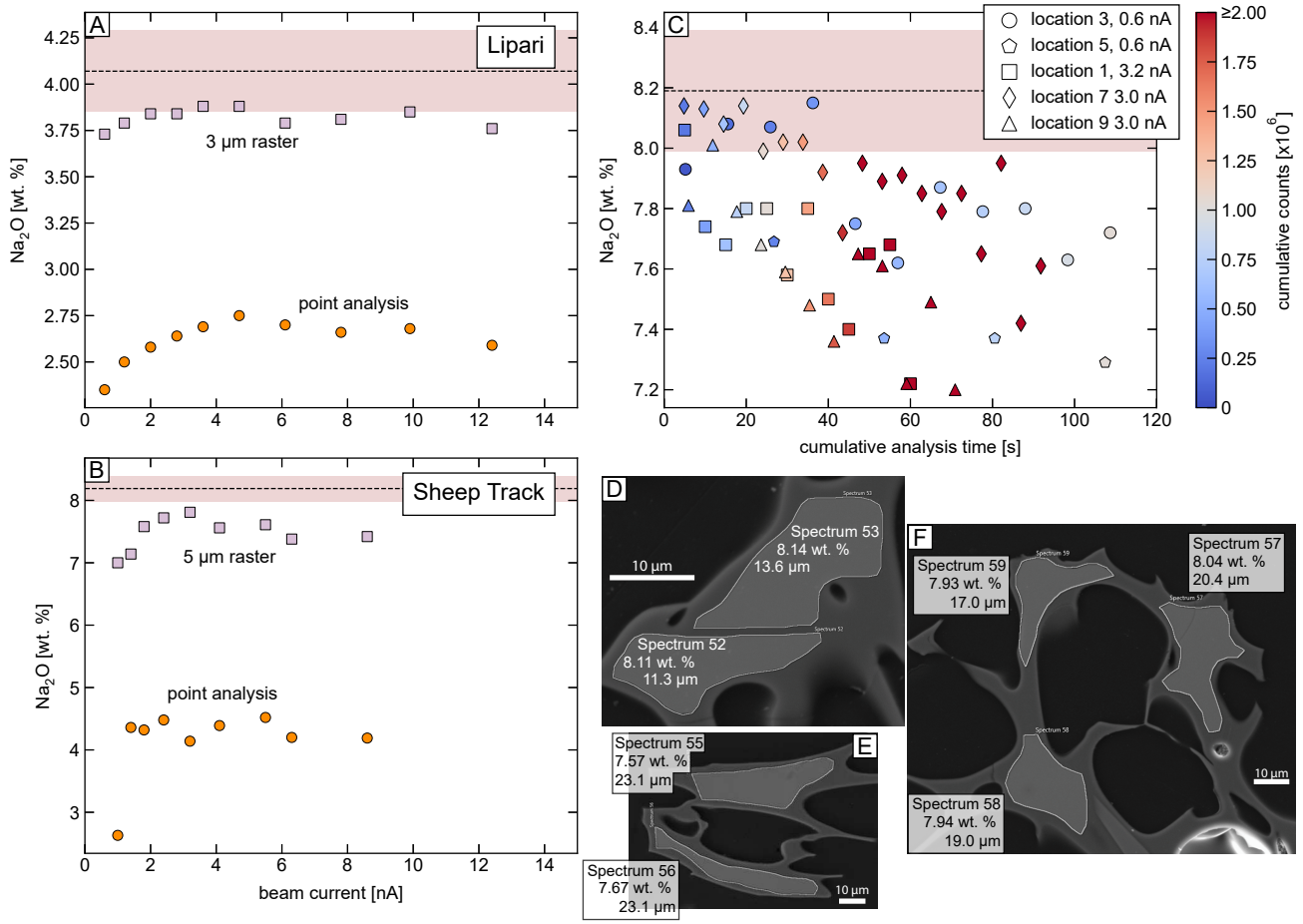


Figure 9: Summary of the optimization steps for the analysis of the Sheep Track tephra. [A, B] The analysis of Lipari and Sheep Track, respectively, over a range of currents. Both reach a maximum Na_2O concentration at a moderate beam current reflecting the optimization of current and counting time in mitigating Na mobility. [C] The cumulative Na loss in Sheep Track tephra due to the repeated analysis of the same 11.6 µm × 8.8 µm field of view. [D–F] Secondary electron images of Sheep Track shards ([E] is rotated 90° from the analysis orientation) showing how the freehand "point and shoot" tool can be used to analyze irregular areas larger than possible using a rectangular or elliptical raster or a defocused electron beam. Each spot is annotated with the measured Na_2O concentration (expected = 8.19 wt.%) and square equivalent length (the square root of the area). These analyses were performed at 15 kV, 3–3.2 nA and collected a spectrum of 0.25×10^6 counts during an analysis time of 6 s. The lower Na_2O concentrations of spectra 55 and 56 [E] indicate heterogeneity of the standard material or of its response to the electron beam. See text for additional details.

5 Reproducibility of glass standards

Similar to the mineral standards (Figure 7), the overall precision and accuracy of the glass measurements are comparable to EPMA data (Figure 10). The rpd of most major elements is <2% and all are <5%. Half of the glass reference materials produced an rpd for K_2O between 2% and 5%, suggesting that our K_2O calibration may be slightly mismatched for these materials. The accuracy of the minor elements follows a similar trend to the mineral standards with nearly all oxides in concentrations 0.1–1 wt.% yielding an rpd <30%. The data are similarly precise, all oxides >10 wt.% have an rsd <2% with most <1%. Likewise, most elements with concentrations between 1 wt.% and 10 wt.% yield an rsd <2% and nearly all <5%. All but one minor element concentrations >0.2 wt.% produces an rsd better than 30%. Unlike for several mineral phases, discussed above, we did not find any significant degradation in the accuracy of the glass measurements performed with a process time of 3 µs (sp 4) versus 16 µs (sp 6). The accuracy and precision of the major and minor oxide compositions are consistent with those reported by 26 EPMA labs that participated in the volcanic glass intercomparison study of Kuehn et al. [2011] for expected concentrations as low as 0.03 wt.% (Figure 10).

6 Limit of detection

The detection limit of SEM–EDS analysis can vary widely based on the analytical parameters, particularly the spectrum counts (and by extension the analysis time), element of interest, and sample matrix. Guyett et al. [2024] estimated a detection limit of approximately 0.2 wt.% (for 1×10^6 count spectra) based on the departure from a power-law relationship between the rsd and expected concentration of glass standards.

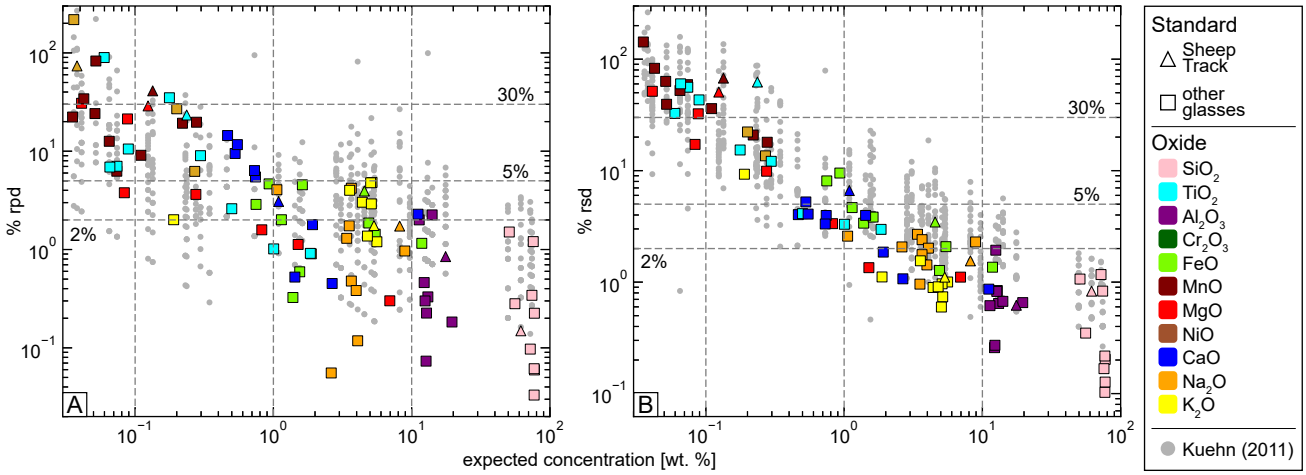


Figure 10: Summary of the accuracy and precision of glass analyses for which Na-loss was successfully mitigated. The triangles are the Sheep Track tephra and squares are all other glass standards (Table 1). The symbol fill color indicates the oxide. [A] The relative percent difference (rpd = 100 × |measured − expected|/expected) compared to the expected concentrations. [B] The relative standard deviation (rsd = 100 × standard deviation/mean) of the measurements. The data for the Panum obsidian and interlab [A–D] are plotted normalized to 100% for consistency with the expected concentrations. The gray circles show the accuracy and precision of the 26 electron microprobe labs that participated in the volcanic glass intercomparison study of Kuehn et al. [2011] illustrating that our scanning electron microscope-energy dispersive spectrometry method achieves comparable data quality.

On the other hand, Newbury and Ritchie [2015] estimated limits of detection of 0.000 04–0.000 25 wt.% (40–250 ppm) for trace elements in the National Institutes of Standards and Technology (NIST) standard reference material (SRM) K497 standard glass for an 87×10^6-count spectrum. They used the NIST SRM K496 standard glass, which has a nearly identical major element composition to K497 but does not contain the trace elements of interest, to estimate the background for K497 analysis, then calculated the detection limit in concentration units (C_{DL}) by:

$$C_{DL} = \frac{3N_B^{1/2}}{N_S - N_B} C_S \quad (1)$$

where N_B and N_S are the measured intensities of the background and peak, respectively, and C_S is the expected or measured concentration. We do not have suitable materials to replicate the approach of Newbury and Ritchie [2015] and the background calculated by OIA is not readily available to the user. Accordingly, we estimated a background for selected spectra using the NIST DTSA-II program [Ritchie 2023] and estimated detection limits from the peak and background intensities using Equation 1. For spectra collected at our standard conditions (15 kV, process time of 16 µs, beam current of approximately 3 nA, and 1.5×10^6 spectrum counts), the detection limits for Ca $K_{\alpha 1}$ and lower energy (≤3.69 keV) peaks were 0.04–0.08 wt.% while higher energy peaks were 0.09–0.19 wt.%. The rsd maintains a negative power law relationship with the expected concentration to as low as 0.03 wt.%, including for higher energy peaks such as Mn (Figures 7 and 10), broadly consistent with our estimates from the peak and background intensities, and suggests that the peak and background intensities we measured with DTSA-II may somewhat overestimate the detection limit for higher energy peaks.

As expected, the detection limits improve with the spectrum counts. For the chromium augite standard the detection limits calculated using 2.5×10^6 count spectra are 2.5–3 times lower than those of the 0.25×10^6 count spectra, and display diminishing returns with increasing counts as was found for the accuracy of the analysis (Figure 1). Detection limits for routine EPMA–WDS analysis focused on major and minor elements are typically 0.01 wt.%, and high current, long analysis time routines for the analysis of trace elements can achieve detection limits as low as 0.000 01 wt.% [10 ppm; e.g. Sobolev et al. 2005; Jercinovic et al. 2012]. Thus, while EPMA–WDS analysis maintains a demonstrated advantage in detection limit, our results and the work of others on the EDS analysis of trace elements demonstrate that the typically assumed order-of-magnitude advantage for EPMA–WDS [e.g. Reed 2005] is overstated.

7 Summary and Prospects

The analytical approach presented here demonstrates the viability of SEM–EDS analysis as a routine quantitative tool for volcanology and the geosciences more generally. The lower acquisition and upkeep costs and the simpler maintenance and operation of SEMs relative to EPMA has great potential to increase the accessibility of quantitative in situ analysis. We do not, however, imagine that the SEM–EDS method presented here will completely supplant EPMA, instead we view it as a complementary technique whereby more routine analysis can be accomplished by SEM–EDS, reserving EPMA resources for applications that require lower detection limits, work on difficult matrices, enhanced spectral resolution, or more granular control of the spatial resolution offered by a field emission source microprobe. In addition to cost and simplicity advantages, SEM–EDS offers additional flexibility

compared to EPMA for the analysis of hydrous glasses. A range of area scans over a range of currents can quickly be acquired to demonstrate that the steps taken to mitigate Na mobility are successful on a sample-specific basis and the beam may be rastered over areas of varying geometry to accommodate squeezing spots onto constrained locations. Whereas the quality of "standardless" analysis has increased significantly, the acquisition of data suitable for publication nevertheless requires sourcing standards for method verification; accordingly, the marginal effort required for fully standardized analysis is modest, with accompanying gains in accuracy and flexibility.

Author Contributions

Both authors declare no competing financial interests. NLA conceived the work, performed the method optimization tests, and matrix optimizations for pyroxene, Fe–Ti oxides, and glass. HW optimized the analytical approach for olivine and plagioclase. Both authors collected standard data included in this report during work on other projects. NLA wrote the first draft of the manuscript, which the authors revised together.

Acknowledgements

We are grateful to the Smithsonian Institution Department of Mineral Sciences and Britta Jensen for providing reference materials. We thank Matt Loewen for fruitful discussions and the USGS internal review of the manuscript, two anonymous reviewers for constructive comments that improved the manuscript, and editorial handling by Jamie Farquharson. This work was supported by the USGS Volcano Hazards Program and the USGS Volcano Disaster Assistance Program (VDAP). Any use of trade, firm, or product names is for descriptive purposes only and does not imply endorsement by the U.S. Government.

Data Availability

All data supporting this work are available in the supplementary information and archived in a Zenodo repository [Andersen and Winslow 2026].

Copyright notice

© The Author(s) 2026. This article is distributed under the terms of the Creative Commons Attribution 4.0 International License, which permits unrestricted use, distribution, and reproduction in any medium, provided you give appropriate credit to the original author(s) and the source, provide a link to the Creative Commons license, and indicate if changes were made.

References

Allaz, J. M., O. K. Neill, and A. von der Handt (2015). "Focused interest group on microanalytical standards (FIGMAS): Assessing the quality, availability and need for standards in the microanalytical community". *Microscopy and Microanalysis* 21(S3), pages 2019–2020. DOI: 10.1017/s1431927615010879.

Andersen, N. and H. Winslow (2026). *Validation data for a scanning electron microscope-energy dispersive spectrometry (SEM–EDS) method for the analysis of common volcanic phases*. DOI: 10.5281/ZENODO.15399935.

Andersen, N. L., A. E. Dechert, D. C. S. Ruth, M. (Sas, J. Chouinard, and J. Dufek (2025). "The transition from melt accumulation to eruption initiation recorded by orthopyroxene Fe–Mg diffusion timescales in late Holocene rhyolites, South Sister Volcano, Oregon Cascade Range". *Geochemistry, Geophysics, Geosystems* 26(12), e2025GC012256. DOI: 10.1029/2025gc012256.

Carpenter, M. A. and J. D. C. McConnell (1984). "Experimental delineation of the $C\bar{1} \rightleftharpoons I\bar{1}$ transformation in intermediate plagioclase feldspars". *American Mineralogist* 69(1–2), pages 112–121.

Costa, F., T. Shea, and T. Ubide (2020). "Diffusion chronometry and the timescales of magmatic processes". *Nature Reviews Earth & Environment* 1(4), pages 201–214. DOI: 10.1038/s43017-020-0038-x.

Fournelle, J. (2011). "An investigation of "San Carlos olivine": Comparing USNM-distributed material with commercially available material". *Microscopy and Microanalysis* 17(S2), pages 842–843. DOI: 10.1017/s1431927611005083.

Fournelle, J., K. Goemann, and A. von der Handt (2020). "A new Kakanui hornblende for use by EPMA labs". *Microscopy and Microanalysis* 26(S2), pages 2162–2164. DOI: 10.1017/s1431927620020668.

Guyett, P. C., D. Chew, V. Azevedo, L. C. Blennerhassett, C. Rosca, and E. Tomlinson (2024). "Optimizing SEM–EDX for fast, high-quality and non-destructive elemental analysis of glass". *Journal of Analytical Atomic Spectrometry* 39(10), pages 2565–2579. DOI: 10.1039/d4ja00212a.

Harries, D. (2014). "Homogeneity testing of microanalytical reference materials by electron probe microanalysis (EPMA)". *Geochemistry* 74(3), pages 375–384. DOI: 10.1016/j.chemer.2014.01.001.

Helz, R. L., D. A. Clague, L. G. Mastin, and T. R. Rose (2014). *Electron microprobe analyses of glasses from Kīlauea tephra units, Kīlauea Volcano, Hawaii*. US Geological Survey. DOI: 10.3133/ofr20141090.

Iverson, N. A., D. Kalteyer, N. W. Dunbar, A. Kurbatov, and M. Yates (2017). "Advancements and best practices for analysis and correlation of tephra and cryptotephra in ice". *Quaternary Geochronology* 40, pages 45–55. DOI: 10.1016/j.quageo.2016.09.008.

Jarosewich, E., J. A. Nelen, and J. A. Norberg (1980a). "Corrections". *Geostandards Newsletter* 4(2), pages 257–258. DOI: 10.1111/j.1751-908x.1980.tb00273.x.

– (1980b). "Reference samples for electron microprobe analysis". *Geostandards Newsletter* 4(1), pages 43–47. DOI: 10.1111/j.1751-908x.1980.tb00273.x.

Jarosewich, E., A. S. Parks, and L. B. Wiggins (1979). "Microprobe analyses of four natural glasses and one mineral: An interlaboratory study of precision and accuracy". *Smithsonian Contributions to Earth Science* 22, pages 53–67.

Jensen, B. J. L., L. J. Davies, C. Nolan, S. Pyne-O'Donnell, A. J. Monteath, V. Ponomareva, M. Portnyagin, R. Booth, M. Bursik, E. Cook, G. Plunkett, J. W. Vallance, Y. Luo,

L. C. Cwynar, P. Hughes, and D. G. Pearson (2021). "A latest Pleistocene and Holocene composite tephrostratigraphic framework for northeastern North America". *Quaternary Science Reviews* 272, 107242. DOI: 10.1016/j.quascirev.2021.107242.

Jercinovic, M. J., M. L. Williams, J. Allaz, and J. J. Donovan (2012). "Trace analysis in EPMA". *IOP Conference Series: Materials Science and Engineering* 32, 012012. DOI: 10.1088/1757-899x/32/1/012012.

Kuehn, S., D. Froese, and P. Shane (2011). "The INTAV intercomparison of electron-beam microanalysis of glass by tephrochronology laboratories: Results and recommendations". *Quaternary International* 246(1-2), pages 19–47. DOI: 10.1016/j.quaint.2011.08.022.

Lowe, D. J., N. J. Pearce, M. A. Jorgensen, S. C. Kuehn, C. A. Tryon, and C. L. Hayward (2017). "Correlating tephras and cryptotephras using glass compositional analyses and numerical and statistical methods: Review and evaluation". *Quaternary Science Reviews* 175, pages 1–44. DOI: 10.1016/j.quascirev.2017.08.003.

Newbury, D. E. and N. W. M. Ritchie (2015). "Performing elemental microanalysis with high accuracy and high precision by scanning electron microscopy/silicon drift detector energy-dispersive X-ray spectrometry (SEM/SDD–EDS)". *Journal of Materials Science* 50(2), pages 493–518. DOI: 10.1007/s10853-014-8685-2.

– (2019). "Electron-excited X-ray microanalysis by energy dispersive spectrometry at 50: Analytical accuracy, precision, trace sensitivity, and quantitative compositional mapping". *Microscopy and Microanalysis* 25(05), pages 1075–1105. DOI: 10.1017/s143192761901482x.

Oxford Instruments (2023). *AZtecLive*. Version 6.0 SP2. https://nano.oxinst.com/products/azteclive.

Pamukçu, A. S., G. A. R. Gualda, and D. M. Gravley (2021). "Rhyolite-MELTS and the storage and extraction of large-volume crystal-poor rhyolitic melts at the Taupō Volcanic Center: a reply to Wilson et al. (2021)". *Contributions to Mineralogy and Petrology* 176(10), 82. DOI: 10.1007/s00410-021-01840-2.

Pamukçu, A. S., K. A. Wright, G. A. R. Gualda, and D. Gravley (2020). "Magma residence and eruption at the Taupo Volcanic Center (Taupo Volcanic Zone, New Zealand): insights from rhyolite-MELTS geobarometry, diffusion chronometry, and crystal textures". *Contributions to Mineralogy and Petrology* 175(5). DOI: 10.1007/s00410-020-01684-2.

Putirka, K. D. (2008). "Thermometers and barometers for volcanic systems". *Reviews in Mineralogy and Geochemistry* 69(1), pages 61–120. DOI: 10.2138/rmg.2008.69.3.

Reed, S. J. B. (2005). *Electron microprobe analysis and scanning electron microscopy in geology*. Second edition. Cambridge University Press.

Rinaldi, R. and X. Llovet (2015). "Electron probe microanalysis: A review of the past, present, and future". *Microscopy and Microanalysis* 21(5), pages 1053–1069. DOI: 10.1017/s1431927615000409.

Ritchie, N. W. M. (2023). *DTSA-II*. https://www.cstl.nist.gov/div837/837.02/epq/dtsa2/index.html.

Ritchie, N. W. M., D. E. Newbury, and J. M. Davis (2012). "EDS measurements of X-ray intensity at WDS precision and accuracy using a silicon drift detector". *Microscopy and Microanalysis* 18(4), pages 892–904. DOI: 10.1017/s1431927612001109.

Saunders, K., B. Buse, M. R. Kilburn, S. Kearns, and J. Blundy (2014). "Nanoscale characterisation of crystal zoning". *Chemical Geology* 364, pages 20–32. DOI: 10.1016/j.chemgeo.2013.11.019.

Sobolev, A. V., A. W. Hofmann, S. V. Sobolev, and I. K. Nikogosian (2005). "An olivine-free mantle source of Hawaiian shield basalts". *Nature* 434(7033), pages 590–597. DOI: 10.1038/nature03411.

Wilson, C. J. N., S. J. Barker, B. L. A. Charlier, M. L. Myers, and K. F. Hansen (2021). "A comment on: magma residence and eruption at the Taupō Volcanic Center (Taupō Volcanic Zone, New Zealand)—insights from rhyolite-MELTS geobarometry, diffusion chronometry, and crystal textures, by AS Pamukçu et al., Contrib Mineral Petrol 175:48 (2020)". *Contributions to Mineralogy and Petrology* 176(10), 79. DOI: 10.1007/s00410-021-01839-9.

Winslow, H., K. J. Lynn, D. T. Downs, A. Lerner, A. P. Ellis, N. Andersen, A. Nalesnik, and F. A. Trusdell (2025). "Utilizing crystal records to determine the underlying architecture and timescales of magmatic processes during the 2022 Mauna Loa eruption". *Bulletin of Volcanology* 88(1), 5. DOI: 10.1007/s00445-025-01918-w.

Wu, S., A. Audétat, K. P. Jochum, H. Wang, J. Chen, B. Stoll, C. Zhang, Z. Bao, S. Yang, C. Li, X. Wang, C. Xu, L. Xu, C. Huang, L. Xie, Y. Yang, and J. Yang (2022). "Three natural andesitic to rhyolitic glasses (OJY-1, OH-1, OA-1) as reference materials for *in situ* microanalysis". *Geostandards and Geoanalytical Research* 46(4), pages 673–700. DOI: 10.1111/ggr.12449.

Yang, S.-Y., S.-Y. Jiang, Q. Mao, Z.-Y. Chen, C. Rao, X.-L. Li, W.-C. Li, W.-Q. Yang, P.-L. He, and X. Li (2022). "Electron probe microanalysis in geosciences: Analytical procedures and recent advances". *Atomic Spectroscopy* 43(1). DOI: 10.46770/as.2021.912.

Appendix A

In the following tables, we summarize considerations and our approach to designing a quantitative SEM–EDS procedure and the workflow at the instrument. In addition to our in-house testing and the recommendations of our EDS detector manufacturer, our approach was influenced by Guyett et al. [2024], Newbury and Ritchie [2015], and Ritchie et al. [2012] and many of their recommendations are mirrored below.

Table A1: Procedure design considerations.

Parameter	Considerations	Tests and optimizations
Sample preparation	Samples must be flat and polished. Insulating samples should be carbon coated to prevent charging. Other conductive coatings (e.g. gold or other metals) will attenuate X-ray transmission from the sample.	Our final polishing steps are 1 µm diamond and 0.25 µm alumina for both standards and samples; however, a finer polish may be required for the analysis of X-rays with energy <1 keV [Newbury and Ritchie 2015]. We coat our samples with approximately 20 nm of carbon, as measured by a quartz sensor in our carbon coater. Ideally, the standards and samples should be coated with the same thickness of carbon. Thinner coats, e.g. 8–10 nm, are common for general SEM work and are also viable for quantitative EDS analysis. The coat only needs to be thick enough to prevent charging.
Beam stability	An unstable beam current will degrade the accuracy and precision of the analysis	Measure the beam current over time using a probe current detector if available or the count rate on a pure metal standard. We prefer our beam current to vary by <1% per hour. Particularly note the stability after venting the chamber and turning on the beam to evaluate if extra pumping or "warming up" the source are needed. The beam current or proxy should be included in the calculation of results to allow for unnormalized data.
Dead-time	There is a trade-off between increasing count rates (achieved at higher currents) and high dead-times that produce pulse-pileup artifacts and inaccurate results.	Validate any pulse pileup correction by inspecting the corrected and uncorrected spectra for artifacts introduced by the correction and comparing analyses of the same standard at high dead-time, pulse pile up corrected conditions and low dead-time, uncorrected conditions. If pile up correction is not available, evaluate the maximum viable deadtime by inspecting the spectra for pileup artifacts. Decreasing the current, and thereby the count rate, such that the dead-time is <10% is typically sufficient to eliminate pileup artifacts [Ritchie et al. 2012].
Process time	Long process times increase the spectral resolution at the cost of higher dead-times and lower throughput. In general, the process time should be set as low as possible while maintaining the desired data quality.	Collect spectra from standards over a range of process times. We found several standards useful for judging the resolution at different energies: a Mn standard, Mn is commonly used by EDS manufacturers to define the minimum resolution specification of their detectors; a pure element or oxide standard with a prominent, low-energy peak, e.g. <2 keV: pure Si, quartz, MgO, Al_2O_3; and a standard with major element concentrations of elements over a range of eV, e.g. the Kakanui hornblende or VG-2 glass. The resolution of a peak is typically quantified as the full width, half max (FWHM). This can be measured in DTSA-II [Ritchie 2023] if it cannot be readily calculated in the software provided with the EDS detector.

Table A1 continued.

Parameter	Considerations	Tests and optimizations
Total counts/analysis time	The accuracy and precision of an analysis will be improved with more total counts in the spectrum; however, this comes at the cost of longer analysis times and potentially compromising beam-sensitive materials. We found significant diminishing returns beyond 1.5×10^6 total spectrum counts for most elements.	Perform a set of analyses over a range of total spectrum counts (or live times) to assess the effect on the accuracy and precision of the analysis.
Working distance	The detector geometry must be maintained between the standards and unknowns to produce accurate results. Most geometry parameters will be fixed, but the working distance (the distance between the bottom of the column and the focal point of the beam) is often readily changed by adjusting the SEM focus.	Set the working distance based on manufacturer recommendations. Maintain consistent working distance during analytical sessions.
Lateral consistency	The detector collimator limits the distance from the center of the field of view from which X-rays can be quantitatively acquired; this distance is likely smaller than the field of view at low magnification.	Test the count rate on a homogeneous material across a field of view to determine the collimator range. We recommend performing analysis at a high enough magnification such that the field of view is smaller than the optimal collimator field.

Table A2: Analytical workflow considerations

	Consideration	Suggestions
Stage navigation and focus	The working distance must be constant between the standards and unknowns or the accuracy of the analysis will be compromised.	Analytical targets must be in focus to ensure they are at the intended working distance. Focus using the secondary electron image. Focus by adjusting the stage height rather than adjusting the working distance—i.e., bring the sample into the beam focal point rather than moving the focal point of the beam to the sample surface.
Beam measurements	The beam current, or a proxy, is needed to calculate unnormalized results. A stable beam current is needed for accurate analysis	The beam current should be monitored at a frequence appropriate for the observed stability. We measure the current every 20 min until we are satisfied it has stabilized, then every 60–90 min thereafter. Field emission source SEMs may require less frequent beam measurements.
Analytical spots	The locations of analysis may be set either in a point-and-shoot interface or by the measurement of a full field of view at high magnification.	We prefer the point and shoot workflow for speed and flexibility, but the size of the collimator must be taken into consideration when placing spots. For full field of view analysis, many SEMs "overscan" the field of view to avoid image artifacts at the margins. Be aware that the field of view of the image may be smaller than the actual raster area.

Table A2 continued.

	Consideration	Suggestions
Monitor standards	Standards should be run with unknowns to confirm the accuracy of the analysis and monitor for drift.	We prefer to reserve our closest matrix-matched standards for secondary standards rather than using them for calibration. At a minimum, secondary standards should be run at the beginning and end of an analytical session. We typically also run additional standards throughout the session for a total of 6–10 replicates per standard per day
Automation	The extent to which automation can be implemented depends on the capabilities of the instrument software and the accuracy of the stage location recall.	We have found our analytical times to be too short to make automation worthwhile; however, for low dead-time/low current, long analysis time workflows, automation may be more useful.
Beam sensitive material	Glass and some minerals are susceptible to beam damage that can produce spurious results for mobile elements such as Na.	Measuring rasters instead of points can mitigate beam damage; we found 10 µm squares were able to overcome Na-mobility issues in most volcanic glass standards. The success of mitigation efforts can be quickly evaluated on a sample-specific basis by measuring a range of raster sizes and observing if the concentrations of the mobile element converge. We found decreasing the current to be counterproductive below approximately 3 nA as the lower count rates necessitated longer counting times. This point of diminishing returns will likely be lower for larger area detectors and may vary between sample matrices. The current, raster size, and analytical time can be optimized for particularly sensitive samples by comparing measurements over a range of currents and evaluating the change in concentration with progressively longer beam exposure.